Analyst

Accepted Manuscript

This article can be cited before page numbers have been issued, to do this please use: A. A. I. Sina, E. Ahmed, M. K. Masud, Md. S. A. Hossain, J. Na, Y. Yamauchi and M. Trau, *Analyst*, 2020, DOI: 10.1039/D0AN01096K.

ROYAL SOCIETY OF CHEMISTRY

rsc.li/analyst

Nanostructured mesoporous gold electrodes detect protein phosphorylation in cancer with electrochemical signal amplification

Emtiaz Ahmed[a,†], Mostafa Kamal Masud[a,†], Md. Shahriar A. Hossain[a,b], Jongbeom Na[a], Abu Ali Ibn Sina [a,*], Yusuke Yamauchi[a,c,*] and Matt Trau[a,d,*]

[a]*Australian Institute for Bioengineering and Nanotechnology (AIBN), The University of Queensland, Brisbane, QLD 4072, Australia*

[b] *School of Mechanical and Mining Engineering, Faculty of Engineering, Architecture and Information Technology (EAIT), The University of Queensland, Brisbane, QLD 4072, Australia.*

[c]*School of Chemical Engineering, Faculty of Engineering, Architecture and Information Technology (EAIT), The University of Queensland, Brisbane, QLD 4072, Australia.*

[d]*School of Chemistry and Molecular Biosciences, The University of Queensland, Brisbane, QLD 4072, Australia*

**Corresponding authors: a.sina@uq.edu.au, y.yamauchi@uq.edu.au and m.trau@uq.edu.au*

†Equal Contribution

View Article Online
DOI: 10.1039/D0AN01096K

Abstract

Protein phosphorylation is a posttranslational modification of kinase proteins that changes protein's conformation to regulate crucial biological functions. However, phosphorylation of protein is significantly altered during cancer progression which triggers abnormal cellular pathways and can serve as an emergent diagnostic and prognostic biomarker for cancer. Herein, we develop a nanostructured mesoporous gold electrode (NMGE) that enables highly sensitive detection of protein phosphorylation with electrochemical signal amplification. The biosensor comprises nanostructured mesoporous gold electrodes with a superior electro-conductive framework than the nonporous electrodes. We characterize our developed nano/mesoporous gold electrode with various electrochemical methods in the presence of $[Fe(CN)_6]^{3-/4}$ redox system. We find that the mesoporous gold electrode catalyzes both the oxidation and reduction process of $[Fe(CN)_6]^{3-/4}$ system and generates a 3-times higher current signal than the non-porous gold electrode. The superior signal transduction of our nano/mesoporous gold electrode is enabled through pore-induced i) high electrochemically active surface area, and ii) reduced impedance with high signal to noise ratio. The assay utilizes direct adsorption of immunoprecipitated purified BRAF protein towards the mesoporous gold electrode and thus avoids cumbersome sensor surface functionalization. Our developed biosensor detects phosphorylated BRAF protein with 2.5-folds increase in sensitivity and ≈10-folds increase in the limit of detection (LOD) in comparison to the nonporous gold electrodes. The assay also works on a wide dynamic range from 0.5-20 ng/µl of protein which further shows its ability for clinical application. We envisage that this nanostructured mesoporous gold biosensor will be of high interest for clinical application.

Keywords: Nanostructures, mesoporous gold electrode, electro-catalytic activity, protein phosphorylation, electrochemical detection, cancer.

View Article Online
DOI: 10.1039/D0AN01096K

1. Introduction

Protein phosphorylation is one of the most prominent molecular regulatory mechanisms that control almost all aspects of cellular functions.[1-2] Phosphorylation changes protein's structure and conformation and regulates a broad range of cellular activities including the metabolism, cell cycle, differentiation, and apoptosis.[1-4] However, this mechanism is often impaired in cancer by abnormal protein phosphorylation which therefore can be used as a biomarker for early cancer detection and monitoring of therapy response.[5-6] Current standard platforms for detecting and monitoring protein phosphorylation include western blot,[7] intracellular flow cytometry[8] and enzyme-linked immunosorbent assays (ELISA).[9] However, these methods mostly use labelling with phosphospecific antibodies which are expensive and most importantly antibody cross-reactivity between different epitopes of proteins can lead to immune-histochemical artifacts. Mass spectroscopy[10] and protein sequencing[11] can also be used for analyzing protein phosphorylation. However, these methods require expensive instruments and expert handling. A label-free, simple and cost-effective biosensor that can detect protein phosphorylation with high sensitivity may enable routine monitoring of cancer in the clinic.

Mesoporous metal structures have recently attracted great interest in manufacturing solar cells, fuel cells and optoelectronic devices due to their tiny pore size, high surface-to-volume ratio, and intrinsic electrochemical properties.[12-13] However, most mesoporous materials are mainly composed of silica, titania, and other metal oxides, which are usually not very suitable for biosensing applications.[12,14] Recently, Yamauchi *et al.* developed a novel soft-templating method to fabricate mesoporous gold (Au) films with highly controllable pore size.[15] The method utilizes spherical polymeric micelles derived from high-molecular-weight polymers (*e.g.*, diblock or triblock copolymers) as soft-template to precisely control the crystal growth of Au around the template. This enables the synthesis of mesoporous

structures with gold (Au) which is frequently used in biosensing due to its inherent bio-favorability, conductivity, chemical, and physical stability and predominantly bio-inspired unique surface chemistry.

In this study, we develop a nanostructured mesoporous gold electrode-based biosensor to detect phosphorylated protein in cancer with enhanced sensitivity and specificity. The nanostructured mesoporous gold electrodes (NMGE) of our biosensor are made of mesoporous gold (Au) films synthesized using the soft-templating method. We characterize the nanostructured mesoporous gold electrodes with various electrochemical systems using $[Fe(CN)_6]^{3-/4}$ redox molecules. We find that NMGE catalyzes both the oxidation and reduction process of $[Fe(CN)_6]^{3-/4}$ system. Using differential pulse voltammetry, we find that NMGE generates a 3-times higher current signal than non-porous (149.3 *vs.* 49.85 μA). To examine the adsorption capacity of NMGE, we perform cyclic voltammetry (CV) at different concentrations (0.5 mM to 15 mM) of $[Fe(CN)_6]^{3-/4}$ system and find that the porous structure provides a higher surface and adsorption moiety to accumulate the higher amount of redox molecules. We also investigate the electrocatalytic/adsorption activity of our NMGE using chronoamperometry which follows the characteristic Michaelis-Menten equation typically overserved in enzyme catalysis. We find a low Michaelis-Menten constant (K_m^{app}) which further suggests a higher affinity of NMGE to $[Fe(CN)_6]^{3-/4}$ redox molecules.

To demonstrate the application of our nanostructured mesoporous gold electrode-based biosensor, we select BRAF protein which has been found to be abnormally phosphorylated in many cancers.[16] To detect phosphorylation in BRAF proteins, we use a previously developed interfacial biosensing strategy which can detect DNA, RNA and phosphorylated proteins by directly adsorbing them onto the gold surface.[17-20] Our NMGE shows 2.5-folds increase in sensitivity and ≈10-folds increase in the limit of detection (LOD)

in comparison to the nonporous gold electrodes. The assay also shows a wide dynamic range with a protein concentration ranging from 0.5-20 ng/µl. The method is label-free and does not require any amplification, staining or antibody immobilization for protein detection and offers straightforward sample handling and measurement.

2. Experimental

2.1 Reagents and materials

The reagents and chemicals used were of analytical grade unless otherwise stated. Gold(III) chloride, tetrahydrofuran (THF), potassium hexacyanoferrate(II), potassium hexacyanoferrate(III), 10 % fetal bovine serum and phosphate buffer saline (PBS) tablet (0.01 M phosphate buffer, 0.0027 M potassium chloride and 0.137 M sodium chloride, pH 7.4 at 25 ^{o}C) were purchased from Sigma-Aldrich (Australia). Polystyrene–Poly(ethylene oxide) (PS-b-PEO) diblock Copolymer PS-b-PEO were obtained from Polymer Source Inc. (USA). Tris was purchased from VWR Life science (Australia). RPMI 1640 was cultured from Thermo Fisher Scientific USA. NCI-H1666 and HCC827 lung cancer cell lines were purchased from ATCC. All chemicals and reagents were used as received. UltrapureTM DNase/RNase-free distilled water (Invitrogen, Australia) was used throughout the experiments.

2.2 Culture of target cell lines and BRAF protein

Lung adenocarcinoma cell lines NCI-H1666 and HCC827 were cultured in RPMI 1640 (Thermo Fisher Scientific, USA) supplemented with 10 % fetal bovine serum (Sigma-Aldrich, USA), 1% Glutamax (2mM) and 1% antibiotics containing medium and cells were collected from the medium following standard cell culture protocol. The collected cells were washed with phosphate-buffered saline (PBS) and further subjected to protein extraction. Mycoplasma tests were conducted before and after the experiments. After that, in accordance to manufacturer's instructions, the BRAF proteins were immuno-precipitated from the collected H1666 and HCC827 cells regardless of its phosphorylation status using a phospho-

independent anti-BRAF antibody and protein A/G magnetic beads via magnetic purification. The concentration of all the eluted proteins were measured by bicinchoninic acid (BCA) protein assay.

2.3 Fabrication of mesoporous gold electrode

The NMGE was prepared through electrochemical reduction of Au(III) species present in the micelles containing PS-b-PEO block polymers following our previously published report.[15] (Figure 1a). Briefly, 10 mg of PS (18,000)-b-PEO (7,500) (PS-b-PEO) was dissolved in 3 mL of tetrahydrofuran (THF) at 40 °C followed by the addition of 1 mL of ethanol. 40 mM of aqueous $HAuCl_4$ solution were slowly incorporated under constant stirring and 2.5 mL deionized H_2O was then added to form the spherical micelles. The successive addition of aqueous HAuCl4 enabled the formation of spherical micelles of PS-b-PEO based on the less solubility of PS core in the water. The as-prepared micelle solution was used as precursor solution (electrolyte) directly used for electrodeposition. The electrochemical deposition was carried out using a conventional three-electrode system at a constant applied potential of −0.5 V (vs Ag/AgCl) for 1000 s without stirring by using an electrochemical workstation. The electrodeposition was performed in a standard three-electrode cell system with a gold-coated silicon wafer substrate, typical area of 0.09 cm^2 (0.3 cm × 0.3 cm), as the working electrode, Ag/AgCl (saturated KCl) as the reference electrode, and a platinum wire as the counter electrode. The optimal electrodeposition of Au was carried out at room temperature at a constant potential of –0.5 V (vs. Ag/AgCl) for 1,000 s without stirring. After the Au deposition, it is crucial to remove altogether the polymer from the substrate, and it was removed by dissolving the substrate in THF at 40 ^oC followed by rinsing with deionized water. The uniformly distributed mesopores onto the top surface are seen in the scanning electron microscope (SEM) image (Figure S1, *please see ESI*). The SEM image displays the spherical pores of around 20 ± 5 nm with concave exteriors around the mesopores. X-ray

photoelectronic spectroscopy (XPS) was conducted to know the Au oxidation state and surface chemistry (Figure S2, *please see ESI*). A doublet at 87.7 and 84.0 eV were obtained from the high-resolution scan of Au-4f which is separated by 3.7 eV probably because of spin-orbit coupling. This characteristically represents the presence of Au (0) species in NMGE.

2.4 Electrochemical quantification and differentiation of adsorbed protein on the mesoporous gold electrode

5.0 µL of purified protein sample was adsorbed on the mesoporous gold electrode surface for 30 min. After washing (gently) the electrode with PBS (three times), the differential pulse voltammetry (DPV) experiments were recorded at −0.1 to −0.5 V with a pulse amplitude of 50 mV and a pulse width of 50 ms in 10 mM PBS solution containing 2.5 mM [$K_3Fe(CN)_6$] and 2.5 mM [$K_4Fe(CN)_6$] electrolyte solution before and after adsorbing target protein onto the electrode surface. The $[Fe(CN)_6]^{3-/4-}$ redox system provides an electrochemical environment as well as acts as the electrolyte to measure the adsorption competence using Differential Pulse voltammetry (DPV). The mechanism involved herein is the coulombic repulsion between negatively-charged ferrocyanide ions in the buffer and negatively-charged phosphate groups of adsorbed protein present on the electrode surface partially hinder the diffusion of ferrocyanide ions to the electrode surface. As a consequence, Faradaic current signal generates upon the electrode surface, which is proportionally lower than the bare electrode signals as increasing numbers of proteins become adsorbed onto the surface. This event can be simplified as - the greater the protein adsorption is, the larger the relative current signal difference, %ir, with respect to the baseline. The relative DPV current changes (i.e., $\%i_{Relative}$, percent difference of the DPV signals generated for captured protein ($i_{protein}$) with respect to the baseline current (i_{Bare})) due to the adsorption of protein were then measured by using the following equation;

View Article Online
DOI: 10.1039/D0AN01096K

$$\%i_r = \frac{i_{Bare} - i_{protein}}{i_{Bare}} \times 100$$

where i_{Bare} and $i_{protein}$ are current density obtained for bare electrode and electrode after protein adsorption respectively.[21]

3. Results and Discussions

3.1 Assay Principle

The key framework of this study is to develop a nanostructured mesoporous gold biosensor for sensitive detection of protein phosphorylation in complex samples which might be useful for early cancer detection and monitoring therapy responses. Scheme 1 represents the principles of the assay which involve i) NMGE induced electrochemical catalytic signal amplification and ii) NMGE induced enhanced sensitivity for the detection of protein phosphorylation using interfacial biosensing. The NMGEs were prepared by a soft-templating method using block polymeric-micelles (polystyrene-block-polyoxyethylene; PS-*b*-PEO).

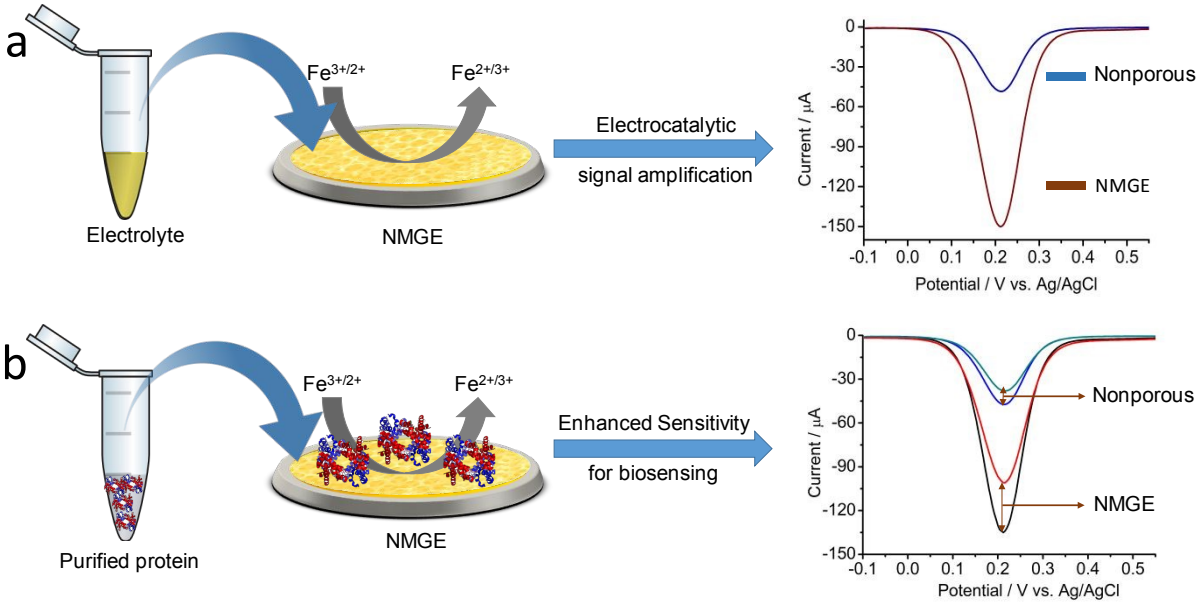

Scheme 1. Nanostructured mesoporous gold biosensor for detecting protein phosphorylation with electrochemical signal amplification. a) NMGE induced electrochemical catalytic signal

amplification b) NMGE induced enhanced sensitivity for the detection of protein phosphorylation using interfacial biosensing.

The polymeric micelles contained the electrochemically reduced Au(III) species and worked as a pore directing agent for forming uniformly sized gold mesopores. The NMGEs were characterized by scanning electron microscope (SEM), X-ray photoelectronic spectroscopy (XPS) and electrochemistry. The SEM image in supplementary figure S1 shows the uniformly distributed spherical pores of around 20 ± 5 nm with the concave framework. XPS analysis in supplementary figure S2 shows the presence of Au(0) in NMGE. The electrocatalytic activity of NMGE was then tested using a number of electrochemical methods.

To detect protein phosphorylation, the target phosphorylated BRAF protein was isolated from lung cancer cell line HCC827 via immunoprecipitation (IP) using magnetic beads. The control non-phosphorylated BRAF protein was isolated from H1666 lung cancer cell line.[22] Generally, the lung adenocarcinoma cell line HCC827 has an acquired mutation in the EGFR tyrosine kinase domain (E746 - A750 deletion) which leads to a constitutively activated EGFR protein.[23] The activated EGFR becomes phosphorylated on tyrosine residues and leads to a cascade of signals transductions,[24] where Ras family protein becomes activated. Activated Ras activates the protein kinase activity of RAF kinase and turns BRAF protein into phosphorylated BRAF (p-BRAF) through sequential chain reactions.[25] In contrary, H1666 cells express wild-type EGFR as well as wild type BRAF proteins).[26] In the next step, the IP-extracted proteins were allowed to adsorb onto the NMGEs for a specific period of time. The average size of the BRAF proteins is ~94 KDa i.e. ~6nm, whereas the pore size of our developed NMGE ranges from 15 to 20 nm which favors the adsorption of proteins onto the NMGE surface.[27] The phosphorylation levels are finally inferred from the total protein adsorption levels, which were quantified electrochemically using Differential

Pulse Voltammetry (DPV) in the presence of $[Fe(CN)_6]^{3-/4-}$ redox system (See Method section for the detail mechanism). We have previously detected protein phosphorylation in EGFR proteins in lung cancer using interfacial biosensing system.[17] Similar to our current assay for BRAF protein, we have previously observed higher adsorption of phosphorylated EGFR protein towards the gold surface in comparison to the non-phosphorylated one. Since phosphorylation can change the conformation of the protein, we hypothesized that phosphorylation might expose the amino-acids with higher gold-affinity (e.g., cysteine) on the protein's surface, or made the protein more hydrophilic that dispersed proteins in solution and allow more interactions with the gold surface. As a result, phosphorylated proteins provided higher adsorption towards the gold surface in comparison to the non-phosphorylated protein.

3.2 Electrocatalytic activity of mesoporous gold electrode towards $[Fe(CN)_6]^{3-/4-}$ redox system

NMGE facilitates increased surface area and geometrical-surface textures that accelerate the redox currents and accessibility of analytes relative to the fine or smooth surface.[28] To check the electro-catalytic activity of our NMGEs, we performed cyclic voltammetry (CV) and measured redox responses of $[Fe(CN)_6]^{3-/4-}$ system. Both the non-porous and mesoporous gold electrode generated a pair of well-defined sharp redox peaks in 2.5 mM $[Fe(CN)_6]^{3-/4}$, giving a reversible single-electron transfer process (Figure 1a and c). The NMGEs provided pointedly higher cathodic (i_{pc}), and anodic (i_{pa}) peak currents in comparison to the non-porous gold electrodes (Figure 1a and b). Notably, i_{pc} increased by approximately 3-times (151.49 *vs.* 49.2 μA) whereas i_{pa} increased approximately 3.6-times (117.5 *vs.* 33.24 μA). Moreover, both E_{pc} and E_{pa} obtained from the CV voltammogram for NMGE experienced a potential shift by 37 mV and 57 mV respectively in comparison to non-porous gold electrode. This data indicates that NMGE catalyzed both the oxidation and

reduction process of $[Fe(CN)_6]^{3-/4}$ system. Moreover, the E_{pa} associated with the reduction of $[Fe(CN)_6]^{3-/4}$ on the mesoporous gold electrode is negatively shifted in relative to that of the non-porous gold electrode, signifying a stronger interaction between the redox system and the NMGE surface.[29] Similar responses were obtained from DPV measurements, where NMGE generated 3-times

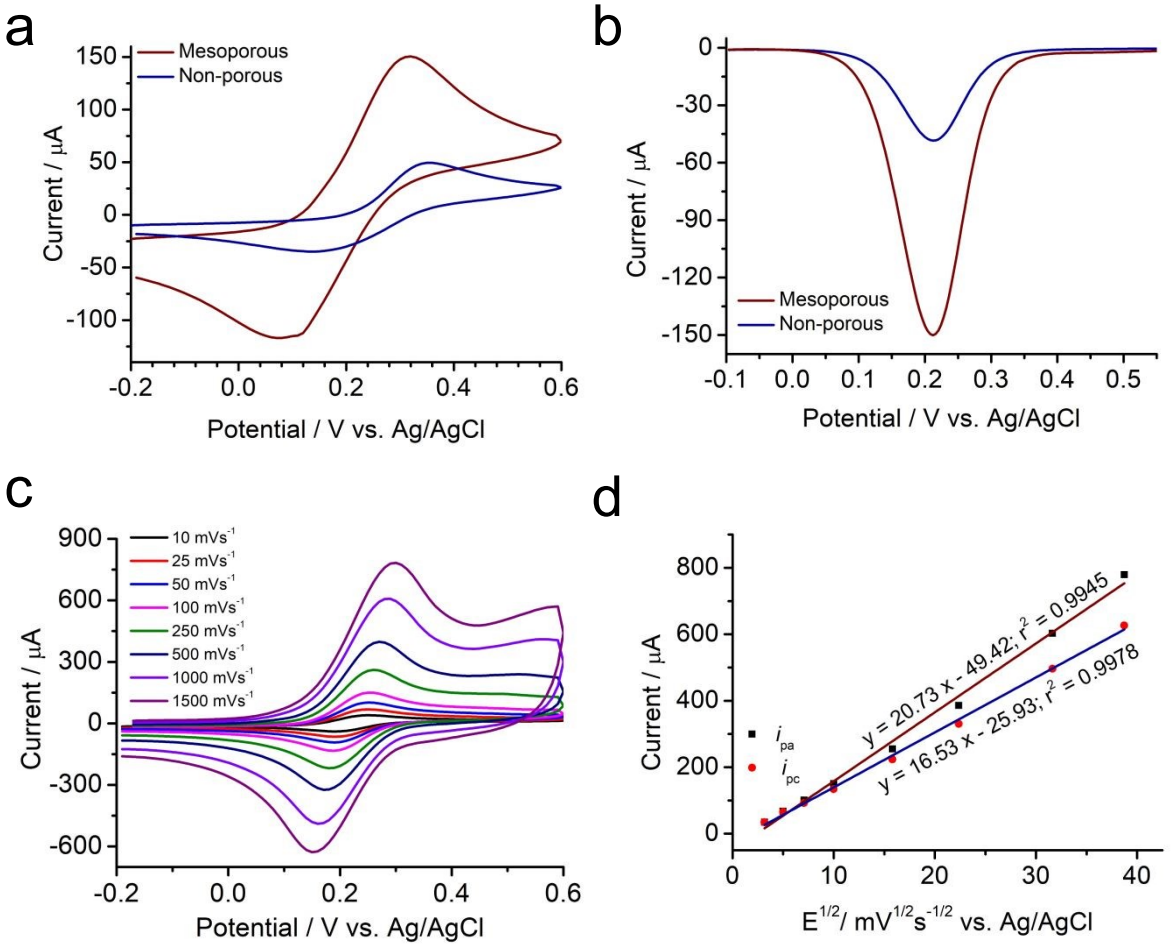

Figure 1. Electrocatalytic activity of NMGE in $[Fe(CN)_6]^{4-/3-}$ redox system. (a) Cyclic voltammogram (CV) of non-porous gold electrode and NMGE, (b) the corresponding bar graph is showing the average cathodic (i_{pc}) and anodic(i_{pa}) peak currents of three replicates. (c) DPV responses between them in 2.5 mM $[Fe(CN)_6]^{3-/4-}$ solution. (d) the corresponding bar graph is showing the average of three replicates. (e) The CV current responses for the scan

rate variation of NMGE (10 mVs^{-1} to 1000 mVs^{-1}) in 2mM $[Fe(CN)_6]^{3-/4-}$ solution, and (f) the corresponding calibration plot are showing the average of three separate trials.

higher current signal than non-porous (149.3 *vs.* 49.85 μA) electrodes (Figure 1c and d). This is due to the mesoporous structure-generated high-surface-area, more exposed-Au surface, pore-induced cascade–catalysis, atomic kink-step sites, and high-index facets present inside the pores. To elucidate the charge transport mechanism involved in the mesoporous gold electrode electro-catalysis towards $[Fe(CN)_6]^{3-/4}$ system, we performed CV measurements of NMGE as a function of different scan rate (Figure 1 e-f). Both i_{pc} and i_{pa} were increasing proportionally with the increased scan rates values (5-1000 mVs^{-1}) and showed a linear relationship with $\nu^{1/2}$ for both i_{pa} and i_{pc}, which indicates the kinetics towards the electrode surface were mainly diffusion-controlled and suggesting electrochemical activity of NMGE towards the $[Fe(CN)_6]^{3-/4}$ system.[20,30] Moreover, the as prepared NMGE showed high stability, providing similar (stable) current responses over the 30 cycles of cyclic voltammetric runs in presence of $[Fe(CN)_6]^{3-/4}$ redox system (Figure S3, *please see ESI*). The higher stability in reaction media and strong affinity towards the redox molecule is highly deliberate for exploiting NMGE as the impeccable signal-transduction for electrochemical biosensing.

3.3 Electrochemical analysis to understand the adsorption capacity of the NMGE

To examine the adsorption capacity of NMGEs, we conducted the CV experiments at different concentration (0.5 mM to 15 mM) of $[Fe(CN)_6]^{3-/4-}$ system. It can be seen from Figure 2a and b, with increasing the redox system both the currents increase gradually, revealing that the porous structure provides higher surface and adsorption moiety to accumulate higher amount of redox molecules. To further investigate the electrocatalytic adsorption activity, chronoamperometric (CA) responses of NMGE were recorded upon the successive addition of $[Fe(CN)_6]^{3-/4-}$ solution (Figure 2 c-d), where the chronoamperometric

current response first increased steeply. The calibration curve follows the characteristic Michaelis-Menten equation that typically shown by enzyme catalysis. The apparent Michaelis-Menten constant (K_m^{app}) can be obtained from the electrochemical version of Lineweaver-Burk model, and it was estimated to be 1.42 mM. This value is significantly low, suggesting the higher affinity of NMGE to $[Fe(CN)_6]^{3-/4}$ redox system, further verifying electrocatalytic adsorption activity of NMGE.

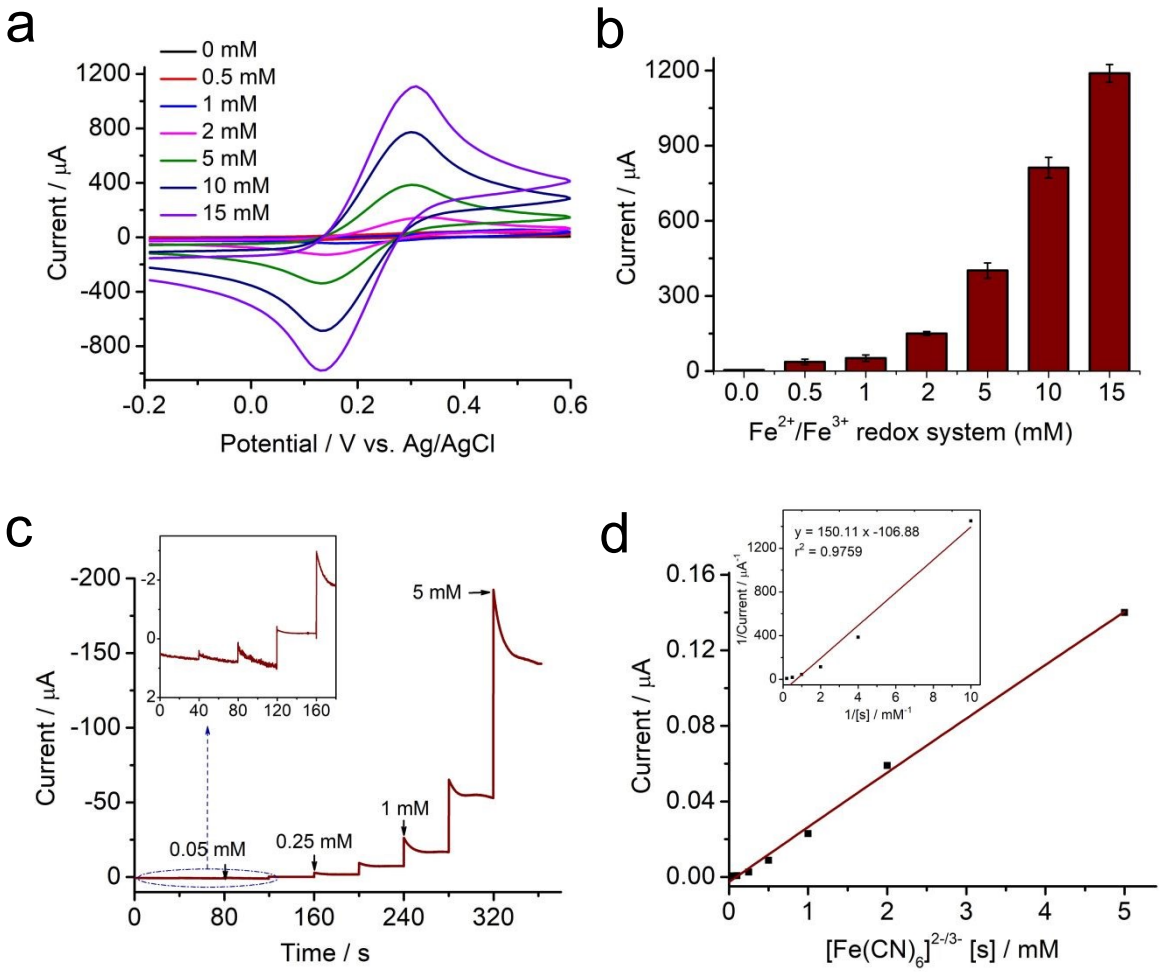

Figure 2. The adsorption capacity of the NMGE. (a) The CV responses at different concentration of $[Fe(CN)_6]^{3-/4-}$ on NMGE and (b) the corresponding bar graphs are showing the average of three separate trials. (c) The amperometric responses of NMGE with the

successive addition of $Fe(CN)_6]^{3-/4-}$ solution (0.05 to 5 mM) into the 0.01M PBS (pH-7). (d) the corresponding calibration plot; *inset- Lineweaver-Burk Model.*

This superior electrocatalytic adsorption activity could be related to its strong electronic field around the center of the uniform mesopores and on the walls between the pores. In addition to this superior activity, the NMGE is advantageous with high stability. The higher adsorption capacity of the NMGE is particularly important for our biosensing assay because interfacial biosensing involves direct adsorption of proteins towards the gold surface. We believe the higher adsorption capacity of NMGE will significantly improve the sensitivity of detection.

3.4 Mesoporous gold electrode-based protein detection using protein-gold affinity interactions

To investigate the applicability of our NMGE biosensor, we decided to detect BRAF protein phosphorylation in cancer. We adsorbed phosphorylated and non-phosphorylated protein onto the NMGE and measured the resulting faradaic current response before and after adsorption by DPV in the presence of $[Fe(CN)_6]^{3-/4-}$ redox system. The concentrations of phosphorylated and non-phosphorylated BRAF proteins extracted from HCC827 and H1666 cell lines respectively were carefully measured with the BCA protein assay reagent and normalized before adsorption. The protein phosphorylation was detected by comparing the adsorption levels of the target p-BRAF proteins against the internal standard control representing the non-phosphorylated isoform (i.e., BRAF). However, the adsorption of protein on NMGE is generally a kinetic process, that's why we first optimized the adsorption time which could play a pivotal role in affinity-based detection approaches. We adsorbed a defined concentration (5 ng/µl) of p-BRAF protein for different amounts of time (*i.e.* 15 min, 30 min, 45 min, 60 min, and 75 min). As can be seen from Figure S4 (*please see ESI*), with

increasing adsorption time, the relative adsorption activities have been increased. However, after 30 min of adsorption (Figure S4b), the polynomial fits show a plateau of relative adsorption. Thus, we choose 30 min incubation for the subsequent experiments as an optimum condition. Next, we investigated the ability of our NMGE biosensor to specifically detect phosphorylation in BRAF proteins. We used non-phosphorylated BRAF and a no-template sample (NoT, PBS is used instead of proteins) as our control samples. As can be seen in figure 3a and b, our NMGE biosensor shows approximately 4.5 and 11 times higher relative adsorption activity for phosphorylated BRAF than the non-phosphorylated and no-template control samples.

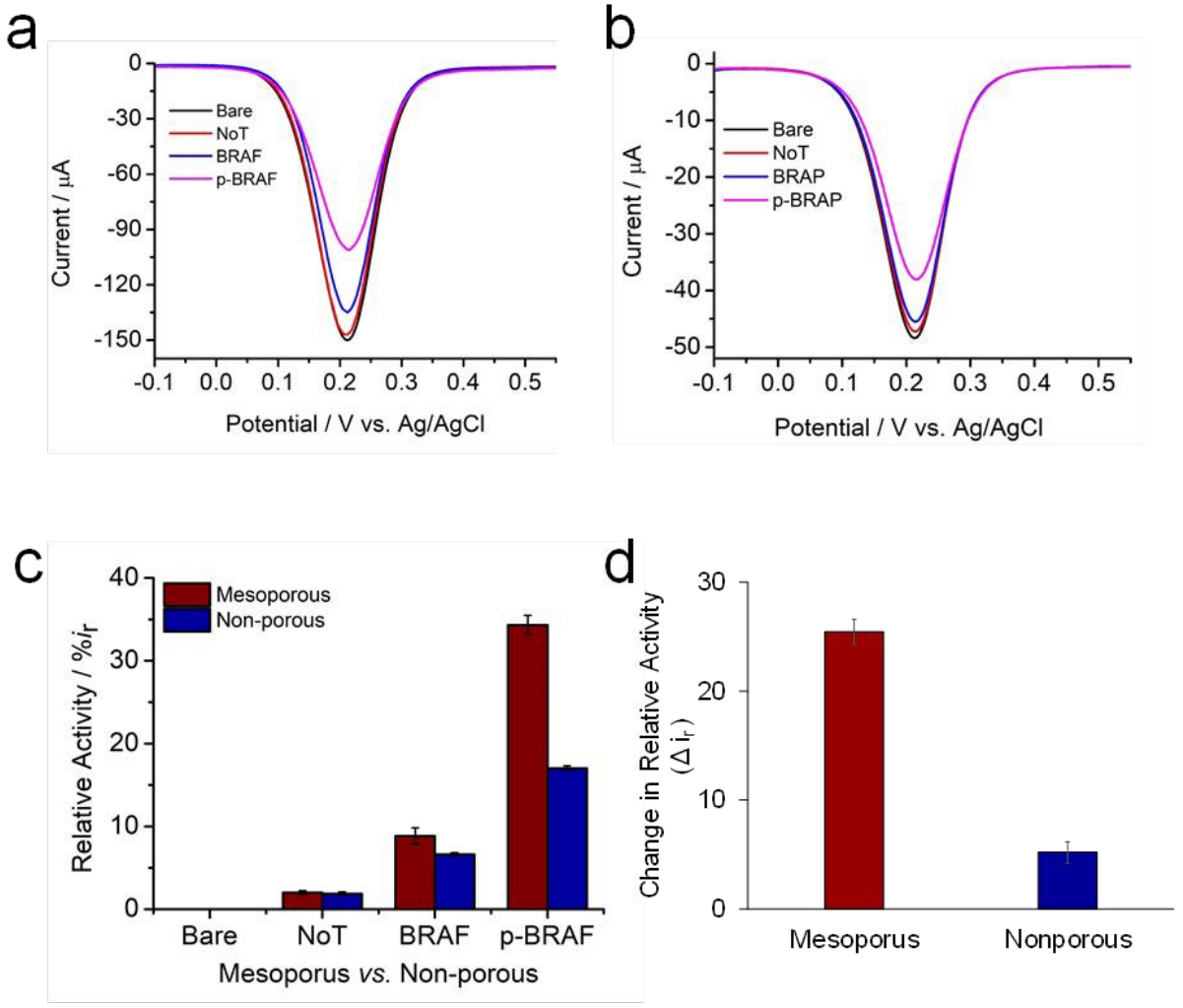

Figure 3. Assay specificity and performance. Figure a and b present the DPV responses of BRAF and p-BRAF along with bare and NoT (PBS is used instead of protein) at NMGE and non-porous gold electrode respectively. Figure c demonstrates the difference in current responses between NMGE and non-porous gold electrode after protein adsorption and the change in relative activity for both BRAF and p-BRAF between NMGE and nonporous electrode is represented in Figure d. Each bar represents the average of three separate trials and the error bars represent the standard deviation of the measurements (% RSD = < 5%, for n = 3).

To investigate the superiority of NMGE over the non-porous gold electrode, we interrogated both p-BRAF and BRAF proteins along with a no-template control (NoT, PBS is used instead of proteins) using nonporous gold electrodes. As can be seen from figure 3 c-d, non-porous gold electrodes show only approx. 2 and 4 times higher relative adsorption activity for the p-BRAF adsorption in comparison to the BRAF and no-template control samples. Our NMGE biosensor showed approx. 2.5 times higher sensitivity than the nonporous gold electrodes in detecting protein phosphorylation. These differences in their respective adsorption trends between mesoporous and nonporous gold electrodes suggest different kinetics and could be associated with differences in their 3D conformation affecting the type of amino acids exposed in the protein's surface and their respective affinities towards the gold surface. These data suggest the superiority and higher specificity of the mesoporous gold electrode for phosphorylated protein detection over non-porous without any prior modification or amplification of target protein.

To determine the dynamic range and limit of detection of the NMGE biosensor, we tested both purified BRAF and p-BRAF proteins with concentrations ranging from 500 pg/µl to 20 ng/µl. The DPV graphs in figure 4 a-b show the representative adsorption pattern of both BRAF and p-BRAF protein with varying concentrations. An increased level of

adsorption represented by decreased DPV signal was observed with increasing protein concentrations. The adsorption levels (% relative activity) for both the BRAF and p-BRAF increases linearly and follows the trend of a straight line. However, as shown in figure 4c-d, each concentration of the p-BRAF exhibits significantly higher responses than the BRAF protein. The linear regression equation for both proteins was estimated, and the limit of detection was also calculated by considering s/n ration equals to three compared to NoT. The NMGE enables a limit of detection of 500 pg/µL (0.5 ng/ µL) for p-BRAF derived from cancer cells with a wide dynamic range of concertation from 0.5 ng/µl to 20 ng/µl. Our NMGE biosensor achieved 0.5 ng/µL sensitivity, whereas the nonporous gold resulted in 5 ng/µL of protein from the same input of the sample. This is an improvement of 10 times in the limit of detection revealing the superiority of porous structure over non-porous gold.

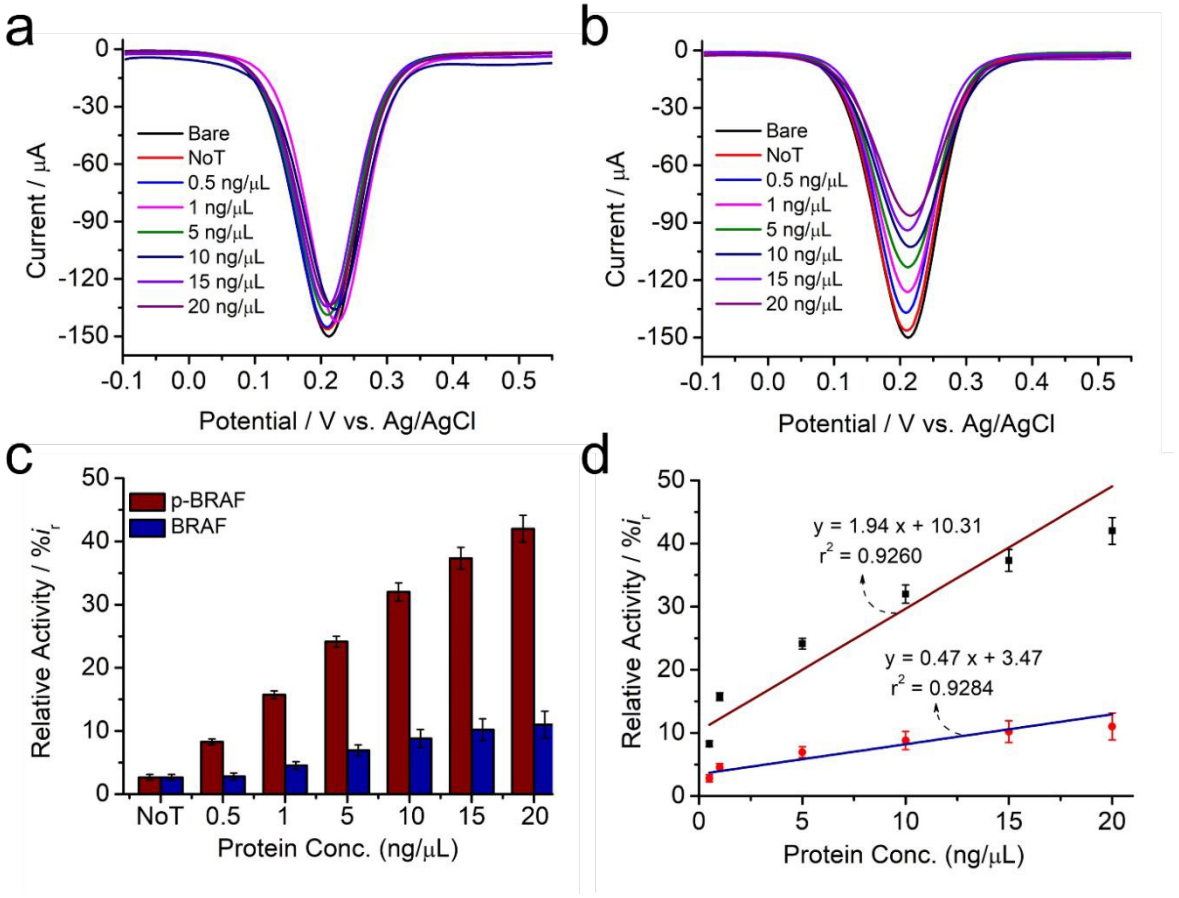

Figure 4. Assay sensitivity. Figure a and b represents the DPV responses with the different concentration of BRAF and p-BRAF ranging from 0.5 to 20 ng/μL respectively. The corresponding bar diagram of assay sensitivity is shown in Figure c (Error bars represent the standard deviation of the measurements (% RSD = < 5%, for n = 3)). The corresponding calibration plot for both BRAF and p-BRAF is depicted in Figure 4d (p-BRAF –red line and BRAF – blue line).

The determination and analysis of protein phosphorylation is an essential component to understand intracellular parameters underlying cellular activities during cancer. Our NMGE based assay showed almost similar or better sensitivity in comparison with recently reported assays. For instance, the NMGE based assay showed 20 times higher detection limit in comparison to the previously reported phosphorylated protein detection technique,[17] which suggests our NMGE biosensor may provide better suitability for clinical application. A detailed comparison of the analytical performances to detect phosphorylated proteins with other recently reported assays are shown in the ESI Table S1. Most of the recently reported techniques detect phosphorylation based on the protein kinase activity which requires previously designed peptides or genetically-encoded probes.[31-34] In comparison to these reports, our NMGE platform is considerably simpler, label-free and faster which does not require any previously designed peptides or genetically-encoded probes. Moreover, our platform is highly versatile and could potentially be applied to any type of protein without any previous knowledge of the target-peptide composition since we specifically avoid the functionalization of sensors with kinase target-specific peptides. This is a crucial advancement as it could even be used for determining the phosphorylation status of proteins where the downstream target is unknown. Although NMGE assay has several advantages over other techniques, it still has some challenges such as it requires pre-isolation of the purified protein by immunoprecipitation to ensure protein specificity.

View Article Online
DOI: 10.1039/D0AN01096K

4. Conclusion

We have developed a new-fashioned and facile electrochemical platform for the highly sensitive detection of protein phosphorylation using interfacial biosensing. Our nanostructured mesoporous gold electrodes based biosensor provided many advantages over nonporous gold electrodes such as *i*) it significantly increased the electrochemically active surface areas and geometrical-surface textures that accelerate the redox currents and accessibility of analyte, *ii*) it decreased the amplitude of the noise and thus achieved high signal-to-noise ratio by lowering the impedance of the electrode, and iii) it provided higher adsorption moiety at the electrode surface to accumulate more molecules. Furthermore, since our NMGE provided a larger surface area through pores, it would be possible to significantly reduce the electrode size, which will enable the placing of multiple electrodes in a high-density array for advanced spatial resolution and multiple sample detection. Our NMGE biosensor showed a significant increase in sensitivity and was able to detect protein phosphorylation from as low as 500 pg/µl of protein which is 10 times higher that it's nonporous counterpart. Overall, our NMGE biosensor has many advantages such as i) it offers single-step detection after isolation of target protein from the complex samples, b) avoids additional modification or functionalization of target protein due to its direct affinity towards the gold surface, c) enables label-free and rapid detection, and d) provides the translation capability for designing portable protein sensor in ill-equipped diagnostic labs, basically in remote areas. We believe that this simple method may potentially provide a clinically applicable platform for protein phosphorylation detection and find a broad spectrum of applications in biotechnology, bioanalysis and clinical diagnosis.

5. Declarations

Conflicts of interest

The authors have no conflict of interests to disclose.

Availability of data and material

All the raw data are available.

Authors Contribution

AAIS, YY and MT conceived the project. AAIS designed the experiments with the assistance YY and of MT. EM and MKM performed most of the experiments. MSH and JN helped with the electrode fabrication. AAIS, EM and MKM wrote the paper with the contribution from all authors.

Funding

This work was supported by NHMRC Investigator Grant (APP1175047 for AAIS), UQ ECR Grant (UQECR1945613 for AAIS) and ARC DP (DP180102836 for MT), ARC DP (DP190102944 for YY). These grants have significantly contributed to the environment to stimulate the research described here. This work was partially supported by the Australian Research Council (ARC) Future Fellowship (FT150100479) to Y. Y. and Australian Government Research Training Program (RTP) Scholarship (The University of Queensland) to M. K. M. The fabrication works were conducted at the Queensland node of the Australian National Fabrication Facility (Q-ANFF).

6. References

1. P. Cohen, *Nat. Cell Biol*., 2002, ***4***, E127-E130.
2. F. Ardito, M. Giuliani, D. Perrone, G. Troiano and L. L. Muzio, *Int. J. Mol. Med*., 2017, ***40***, 271-280.

3. P. Kulkarni, M. K. Jolly, D. Jia, S. M. Mooney, A. Bhargava, L. T. Kagohara, Y. Chen, P. Hao, Y. He and R. W. J Veltri, *Proc. Natl. Acad. Sci*., 2017, ***114***, E2644-E2653.
4. D. Mayer, F. F. Damberger, M. Samarasimhareddy, M. Feldmueller, Z. Vuckovic, T. Flock, B. Bauer, E. Mutt, F. Zosel and J. H. Allain, *Nat. Comm*., 2019, ***10***, 1-14.
5. A. Östman, C. Hellberg and F. D. Böhmer, *Nat. Rev. Cancer,* 2006, ***6***, 307-320.
6. J. S. Sebolt-Leopold and R. Herrera, *Nat. Rev. Cancer*, 2004, ***4***, 937-947.
7. C. W. Lewis, R. G. Taylor, P. M. Kubara, K. Marshall, L. Meijer and R. M. Golsteyn, *FEBS Lett.,* 2013, ***587***, 3089-3095.
8. G. Uzel, D. M. Frucht, T. A. Fleisher and S. S. M. Holland, *Clin. Immunol*., 2001, ***100***, 270-276.
9. J-M. Kee, R. C. Oslund, D. H. Perlman and T. W. Muir, *Nat. Cell. Biol*., 2013, ***9***, 416.
10. S. B. Ficarro, M. L McCleland, P. T. Stukenberg, D. J. Burke, M. M. Ross, J. Shabanowitz, D. F. Hunt and F. M. White. *Nat. Biotech.* 2002, ***20***, 301-305.
11. C. B. Rosen, D. Rodriguez-Larrea and H. Bayley. *Nat. Biotech*., 2014, ***32***, 179.
12. Y. Ye, C. Jo, I. Jeong, J. Lee, *Nanoscale*, 2013, ***5***, 4584-4605.
13. E. J. Crossland, N. Noel, V. Sivaram, T. Leijtens, J. A. Alexander-Webber and H. J. Snaith, *Nature*, J-M. Kee, R. C. Oslund, D. H. Perlman and T. W. Muir, *Nat. Cell. Biol*., 2013, ***9***, 416, ***495***, 215-219.
14. R. Zhang, A. A. Elzatahry, S. S. Al-Deyab and D. Zhao, *Nano Today*, 2012, *7*, 344-366.
15. C. Li, O. Dag, T. D. Dao, T. Nagao, Y. Sakamoto, T. Kimura, O. Terasaki and Y. Yamauchi, *Nat. Comm*., 2015, ***6***, 1-8.
16. C-H. Shen, P. Yuan, R. Perez-Lorenzo, Y. Zhang, S. X. Lee, Y. Ou, J. M. Asara, L. C. Cantley and B. Zheng, *Mol. Cell*, 2013, ***52***, 161-172.

17. M. Ahmed, L. G. Carrascosa, A. A. I. Sina, E. M. Zarate, D. Korbie, K-J. Ru, M. J. Shiddiky, P. Mainwaring and M. Trau, *Biosens. Bioelectron.,* 2017, ***91***, 8-14.

18. A. A. I. Sina, M. T. Foster, D. Korbie, L. G. Carrascosa, M. J. Shiddiky, J. Gao, S. Dey and M. Trau, *Analyst*, 2017, ***142***, 3573-3578.

19. A. A. I. Sina, L. G. Carrascosa, Z. Liang, Y. S. Grewal, A. Wardiana, M. J. A. Shiddiky, R. A. Gardiner, H. Samaratunga, M. K. Gandhi, R. J. Scott, D. korbie and M. Trau, *Nat. Comm.,* 2018, ***9***, 1-13.

20. M. K Masud, M. N. Islam, M. H. Haque, S. Tanaka, V. Gopalan, G. Alici, N-T. Nguyen, A. K. Lam, M. S. A. Hossain, Y. Yamauchi and M. J. A. Shiddiky, *ChemComm*., 2017, ***53***, 8231-8234.

21. A. A. I. Sina, S. Howell, L. G. Carrascosa, S. Rauf, M. J. A. Shiddiky and M. Trau, *ChemCommun.*, 2014*,* ***50***, 13153-13156.

22. B. Sen, S. Peng, X. Tang, H. S. Erickson, H. Galindo, T. Mazumdar, D. J. Stewart, I. Wistuba and F. M. Johnson, *Sci. Transl. Med.*, 2012, ***4***, 136ra70-136ra70.

23. C. H. Yang, H. C. Chou, Y. N. Fu, C. L. Yeh, H. W. Cheng, I. C. Chang, K. J. Liu, G. C. Chang, T. F. Tsai, S. F. Tsai and H. P. Liu, *Biochim. Biophys. Acta Mol. Basis. Dis.*, 2015, ***1852***, 1540-1549.

24. M. R. Meyer, C. F. Lichti, R. R. Townsend and A. G. Rao, *Biochemistry*, 2011, ***50***, 2170-2186.

25. J. Avruch, A. Khokhlatchev, J. M. Kyriakis, Z. Luo, G. Tzivion, D. Vavvas and X. F. Zhang, *Recent Prog. Horm. Res.*, 2001, ***56***,127-155.

26. T. Shimamura, A. M. Lowell, J. A. Engelman and G. I. Shapiro, *Cancer Res.*, 2005, ***65***, 6401-6408.

27. T. Yokota, *Anticancer Agents Med Chem.*, 2012, ***12***, 163-171.

28. L. Soleymani, Z. Fang, E. H. Sargent and S. O. Kelley, Programming the detection limits of biosensors through controlled nanostructuring. *Nat. Nanotech*., 2009, ***4***, 844.

29. C. Li, B. Jiang, H. Chen, M. Imura, L. Sang, V. Malgras, Y. Bando, T. Ahamad, S. M. Alshehri, S. Tominaka and Y. Yamauchi, *Nano Research.,* 2016, ***9***, 1752-1762.

30. M. N. Islam, M. K. Masud, N. T. Nguyen, V. Gopalan, H. R. Alamri, Z. A. Alothman, M. S. A. Hossain, Y. Yamauchi, A. K. Lam and M. J. A. Shiddiky, *Biosens. Bioelectron.,* 2018, ***101***, 275-281.

31. N. Bhalla, M. Di Lorenzo, G. Pula and P. Estrela, *Sci. Rep.*, 2015, ***5,*** 8687.

32. Y. Wang, W. Qim and Y. Song, *ChemComm.,* 2016, ***52***, 7994-7997.

33. Q. Hu, J. Kong, D. Han, Y. Bao, X. Zhang, Y. Zhang and L. Niu, Talanta, 2020, ***206***, 120173.

34. L. Liu, C. Cheng, Y. Chang, H. Ma and Y. Hao, *Sens. Actuators. B Chem*., 2017, ***248***, 178-186.